ELSEVIER

Precambrian Research 79 (1996) 101–123

Precambrian Research

The Ongeluk basaltic andesite formation in Griqualand West, South Africa: submarine alteration in a 2222 Ma Proterozoic sea

D.H. Cornell [a], S.S. Schütte [b], B.L. Eglington [c]

[a] *Geological Institute, University of Göteborg, S-41381 Göteborg, Sweden*
[b] *Department of Geology, University of Natal, Durban 2000, South Africa*
[c] *EMATEK, Council for Scientific and Industrial Research, Pretoria 0001, South Africa*

Received 25 January 1994; revised version accepted 1 December 1995

Abstract

The Ongeluk lavas form part of the Palaeoproterozoic Transvaal–Griqualand West supracrustal sequence of the Archaean Kaapvaal Craton of South Africa. They form a thick shallow-marine volcanic sequence of pillow lava, massive flows and hyaloclastite, which together with their comagmatic subaerial Hekpoort correlate, once covered most of the Craton. In this study the magmatic composition and alteration features of Ongeluk samples were distinguished using geochemistry and radiogenic isotopes.

The Ongeluk–Hekpoort magma was a basaltic andesite derived from anomalous Kaapvaal Craton lithosphere, with a long history of high U/Pb, high Rb/Sr and CHUR-like Sm/Nd ratios. Little evidence for magmatic fractionation was found, although contamination of the lower lavas with Cr-rich material is evident in both Hekpoort and Ongeluk sequences.

The alteration of Ongeluk lavas is characterised using diagrams which compare pillow core–rim pairs, hyaloclastite and massive lava samples with the estimated original magma composition. Alteration is ascribed to a shallow (< 400 m) marine process with both high- and low-temperature stages. This has some common features, but differs in several respects from modern ocean-floor alteration. $^{87}Sr/^{86}Sr$ ratios decreased from magmatic 0.7071 towards seawater 0.7025 during submarine alteration; the Rb/Sr system also reveals a much later ($\sim$ 1200 Ma?) phase of Ca and Rb mobility in a few samples. In contrast the submarine alteration affected Pb isotope ratios so little that a 2222 ± 13 Ma isochron age is regarded as a refinement of earlier dates for the Ongeluk–Hekpoort extrusion. The Ongeluk hyaloclastites acted as a sink for K and Rb in the overlying sea, while the Mn and Ca entering the sea could have contributed to the overlying Kalahari manganese deposits.

1. Introduction

Rocks of the Late Archaean ($\sim$ 2600) to Palaeoproterozoic ($\sim$ 2100 Ma) Transvaal and Griqualand West Sequences form extensive outcrops on the Kaapvaal Craton in southern Botswana and South Africa as shown in Fig. 1. A stratigraphic column and geological map for the Griqualand West portion of the greater Transvaal Basin is given in Table 1 and Fig. 2. For reviews of previous work and stratigraphic subdivisions see SACS (1980, p. 211), Beukes and Smit (1987) and other papers in this special issue. The Ongeluk lavas which occur near the top of the sequence are stratigraphically equivalent to the Hekpoort Basalt Formation of the Transvaal (SACS, 1980) and the Ditlhojana Vol-

SSDI 0301-9268(95)00090-9

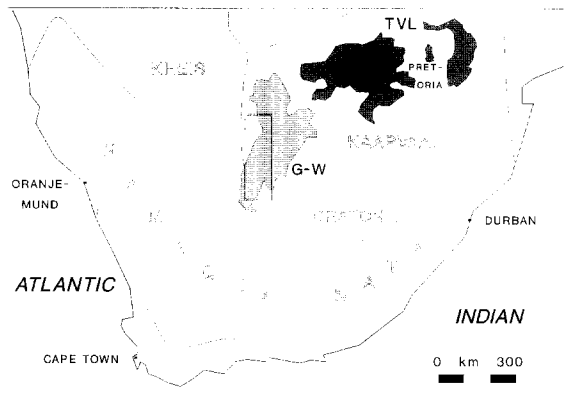

Fig. 1. The outcrop regions of the Griqualand West (*G-W*) and Transvaal (*TVL*) Supergroups are shown in the context of Precambrian structural provinces of southern Africa. The locality of the geological map of Fig. 2 is indicated.

canics of Botswana (Key, 1983); however, large facies changes complicate the correlation of the sedimentary components of the two preserved basins.

In this work we show that the volcanic rocks of the Ongeluk Formation have been affected by seafloor alteration processes analogous to but not identical with spilitization as recognized in Phanerozoic submarine lavas. We characterise the alteration and look through it to establish the primary geochemical and isotopic character and age of the Ongeluk magma.

2. Geological setting

As shown in Table 1, the Griqualand West Sequence (SACS, 1980) comprises mainly chemogenic sediments with clastic sedimentary units and magmatic intercalations, deposited in Palaeoproterozoic times on the structurally stable Kaapvaal Craton. The sequence is almost undeformed and hardly metamorphosed, with igneous minerals still preserved at most localities. The Ongeluk Formation is a thick succession of lavas which crops out over a large portion of the region shown in Fig. 2. The formation thickness is poorly constrained between 300 and 900 m.

Some 160 samples were taken to cover the entire Ongeluk outcrop area shown in Fig. 2, of which 120 were chemically analysed. Some of the best exposures are found in road cuttings along the Griqua-

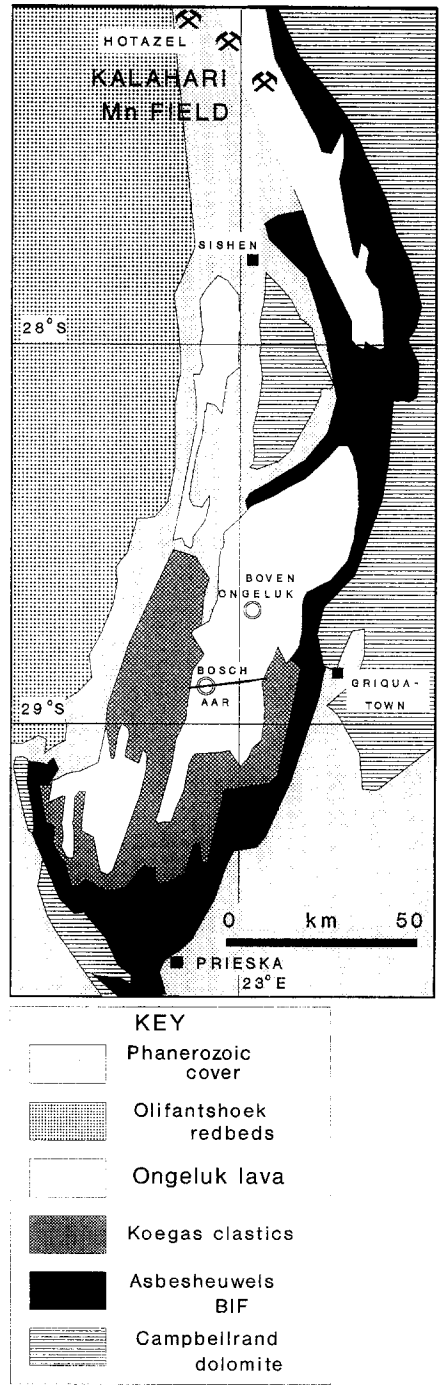

Fig. 2. Geological map showing exposures of Ongeluk lava in the Griqualand West Sequence, and some sample localities of this work.

town–Groblershoop road, notably at Bosch Aar as described by Grobler and Botha (1976). Some sample localities are shown in Fig. 2, a full dataset is available from the first author.

Ongeluk lava samples from the Kalahari Manganese field were found to differ in several respects from the 'regional' Ongeluk discussed in this work. These differences and their genetic relationship to the manganese ore will be described elsewhere.

3. Analytical methods

Whole-rock analyses were done using an X-ray fluorescence spectrometer equipped with a Mo-Sc target X-ray tube, by the method of Norrish and Hutton (1969) for major elements, while trace elements were determined on pressed-powder pellets. Analyses were calibrated using a variety of international rock standards. The dichromate titration method was used for FeO determinations. Representative major and trace element analyses are given in Table 2 and CIPW norms are presented in Table 3. Full analytical data are available on request from the second author.

Electron probe analyses were done using a Cameca instrument at the University of Cape Town, and XRD powder diffractograms were made using a Philips diffractometer with a Co tube.

Rare earth elements were determined with an ICP-AES at the University of Stellenbosch as described by Schade et al. (1989), and by ICP-MS at the University of Natal. Pb and Sr isotope analyses were carried out using a VG 354 mass spectrometer at the CSIR, Pretoria as described by Harmer and Sharp (1985) and Eglington and Kerr (1989). Sm–Nd analyses were made at the Open University, UK, as described by Cornell et al. (1986). Isotope regressions were done using the GEODATE program of Eglington and Harmer (1991), and all age uncertainties are given at the 2σ or 95% confidence level, based on the precision determined at the CSIR from 60 replicate analyses of the same standard.

4. Petrography and mineral chemistry

The Ongeluk Formation comprises essentially three volcanic rock types: massive lava, hyaloclastite and pillow lava.

Table 1
Simplified stratigraphic column for the Griqualand West Sequence after Beukes and Smit (1987)

SEQUENCE		FORMATION	AGE Ma	ROCK TYPES	THICKNESS
OLIFANTSHOEK	Volop	4 Formations		quartzite, greywacke	3500
		Hartley	1928	lava with tuff and breccia	700
		Lucknow		quartzite, subordinate dolomite	450
		Mapedi (≈ Gamagara)		shale, with lava and quartzite bands	10–1500
GRIQUALAND WEST	Voëlwater	Mooidraai (laterally into Beaumont)		dolomite, chert, banded jasper & lava	≈ 250
		Hotazel		banded jasper, dolomite, banded iron and Mn formation	
		Ongeluk Andesite	2222	basaltic andesite massive lava, pillow lava, hyaloclastite	300–900
		Makganyene diamictite		diamictite, minor banded jasper	50–150
	Koegas	6 Formations		iron-formation, shale, quartz wacke, riebeckitic slate	640?
	Asbesheuwels/ Asbestos Hills	Griquatown		clastic-textured iron-formation	200–300
		Kuruman	2432	banded iron-formation	150–750
	Campbellrand	8 Formations	2545	dolomite, subordinate limestone and shale	1500–1700
	Schmidtsdrif	3 Formations		quartzite, subordinate shale, dolomite, limestone, lava	10–250

4.1. Massive lava

Dark-green fine-grained massive lava flows which often show a prominent polygonal joint pattern are the most prominent rock type. Up to 27 flows can be distinguished on aerial photographs, forming prominent scarps separated by less resistant pillow lava and hyaloclastite.

The basal portion of each two to three metre-thick flow tends to be free of amygdales which become more abundant towards the top. Flow breccias are often found near the top of the flow. Well-preserved primary textures are common in thin section. Massive lavas consist of a glassy matrix, now mainly chlorite, enclosing needles of clinopyroxene and plagioclase as shown in Fig. 3. Microprobe analyses of pyroxenes given in Table 4, correspond to augite, which are hollow due to rapid growth. Plagioclase compositions vary, probably due to alteration, the most calcic being An_{56} (Schütte, 1992). Secondary minerals such as quartz, epidote, altered feldspar, zeolites, chlorite and actinolite are commonly found in the matrix and as amygdale fillings. Chlorite pseudomorphs after clinopyroxene are occasionally

Table 2
Chemical analyses of selected samples from the Ongeluk Formation

Sample:	77392 massive lava	77396 chilled flow margin	77397 massive lava	77394 pillow core 77393	77393 pillow rim	88BA6 pillow core 88BA8	88BA8 pillow rim	90BA20 pillow core 90BA19	90BA19 pillow rim	77395 hyalo-clastite	88BA5 hyalo-clastite	90BA28 hyalo-clastite	Detection limit
SiO_2	54.67	54.12	53.21	51.06	54.19	54.96	54.20	52.41	51.89	54.97	53.68	49.76	0.06
TiO_2	0.56	0.66	0.64	0.61	0.72	0.64	0.63	0.64	0.67	0.58	0.60	0.62	0.02
Al_2O_3	14.33	13.58	14.13	13.48	14.03	13.36	14.26	14.52	14.98	13.07	14.46	14.63	0.03
Fe_2O_3(T)	10.33	11.35	10.03	10.12	10.25	11.44	10.31	10.09	11.13	12.76	11.35	14.60	0.02
Fe_2O_3	2.63	2.19	2.53	2.66	2.35	–	–	–	–	2.56	–	–	–
FeO	6.93	8.24	6.75	6.71	7.11	–	–	–	–	9.18	–	–	–
MnO	0.14	0.13	0.13	0.16	0.11	0.14	0.12	0.15	0.14	0.10	0.09	0.11	0.01
MgO	5.75	6.90	5.79	6.08	6.64	6.71	5.96	5.73	6.22	7.48	6.22	8.65	0.09
CaO	7.96	5.30	9.00	12.17	3.92	5.56	6.51	9.76	7.43	4.46	6.55	4.14	0.01
Na_2O	2.64	2.02	2.52	2.58	3.95	3.69	4.03	3.89	2.45	0.17	0.03	0.06	0.09
K_2O	0.32	2.21	0.77	0.00	0.38	0.33	1.33	0.18	0.93	1.49	2.04	1.91	0.01
P_2O_5	0.08	0.09	0.08	0.12	0.12	0.10	0.11	0.11	0.12	0.07	0.08	0.09	0.01
H_2O	0.34	0.24	0.29	0.18	0.27	0.16	0.20	0.00	0.00	0.25	0.57	0.00	–
L.O.I.	4.11	4.15	3.81	3.69	3.82	3.00	2.70	2.79	3.75	6.05	4.53	5.53	–
Total	100.46	99.83	99.65	99.50	97.61	100.09	100.36	100.27	99.71	100.43	100.20	100.10	
V	202	200	211	207	223	218	221	196	210	195	187	194	1
Cr	176	88	88	80	98	92	88	93	99	85	78	106	1
Ni	72	82	81	82	84	96	86	80	86	81	76	94	1
Cu	63	45	68	69	35	65	72	59	48	48	59	56	1
Zn	69	67	76	66	64	92	67	56	90	73	61	85	2
Ga	11	6	8	15	8	11	14	18	18	7	15	18	1
Rb	14	90	34	3	22	13	52	6	35	56	69	64	3
Sr	216	78	172	30	70	104	144	89	186	15	16	21	3
Y	23	21	22	24	22	23	23	20	20	18	17	17	3
Zr	110	111	105	101	116	108	106	91	94	93	88	84	3
Nb	7	6	6	5	6	6	6	4	4	6	4	5	4
Ba	141	519	360	51	188	124	461	58	380	–	279	304	4
Pb	< 4	< 4	4	9	< 4	5	6	4	6	6	7	12	4
Th	7	7	9	7	7	6	7	5	6	< 5	6	5	5
U	< 9	< 9	< 9	< 9	< 9	< 9	< 9	< 9	< 9	< 9	< 9	< 9	9

Sample 77392 is from a road cutting on farm Vannelsdam, the others are all from the large cutting on farm Bosch Aar, on the Griquatown–Groblershoop road; lat. 28°53.8′S; long. 22°48.6′E. Where two samples are from the same pillow, the associated sample number is given second; – = not determined; accuracy is better than 3% relative for major elements above 10 wt% and for trace elements above 100 ppm.

Table 3
CIPW norms for average analyses of different subsets and rock types in the Ongeluk Formation

	Selected dataset	Regional Ongeluk	Kalahari Ongeluk	Pillow cores	Pillow rims	Hyaloclastite	Hekpoort lavas
Qz	8.05	8.58	12.20	4.97	4.82	18.00	13.08
Co	0.00	0.00	2.84	0.00	0.00	2.41	0.00
Or	3.66	4.49	11.76	1.48	4.14	10.58	4.73
Pl	48.79	47.40	34.67	50.06	53.37	28.25	45.78
(Ab)	23.44	22.51	17.52	25.72	32.24	0.85	15.48
(An)	25.35	24.89	17.15	24.33	21.13	27.41	30.30
Di	14.50	15.21	0.00	23.40	10.19	0.00	8.10
Hy	20.61	19.87	30.65	15.53	22.68	35.77	24.11
Mt	2.34	2.32	3.27	2.30	2.31	2.91	2.19
Il	1.23	1.23	2.89	1.22	1.25	1.18	1.16
Ap	0.24	0.24	0.54	0.24	0.26	0.19	0.24

seen. Microprobe analyses of chlorite (Schütte, 1992) correspond to pycnochlorite and ripidolite following Hey (1954), and yield formation temperatures of 227° to 264°C using the chlorite geothermometer of Cathelineau and Nieva (1985) as adapted by MacLean and Kranidiotis (1987).

4.2. Pillow lava

Pillow lava is common throughout the Ongeluk Formation, although easily recognized only in fresh outcrop as in Fig. 4. Pillows have very dark-green rims, cooling cracks, and rounded three-dimensional forms, with either vesicular or massive cores. Chert commonly fills tricuspate interstices between pillows and its occurrence is the only good criterion for pillow lava in weathered outcrop, where onion-skin weathering is commonly developed in massive lavas.

4.3. Hyaloclastite

Hyaloclastite consists of fragments of massive lava in a matrix of angular glass shards, as shown in Fig. 5. No graded bedding is observed. Alteration of

Fig. 3. Photomicrograph of massive lava sample NG470 under crossed polars, showing pyroxene needles set in an isotropic glassy matrix, now chlorite. The large straw-like grain is 1 mm long.

hyaloclastite is evidenced by the development of brown palagonite and epidote or piedmontite along shard boundaries, while the matrix now consists largely of zeolites and chlorite. The glassy fragments probably originated during quenching and shattering of the outer parts of pillows, the matrix representing aquagene tuff.

5. Geochemical recognition of alteration

Inspection of the 104 available analyses of 'regional' Ongeluk lava samples (excluding the Kalahari Manganese Field) reveals a far greater diversity than could be attributed to igneous differentiation, which is reflected in the large standard deviations of the average analysis given in Table 5. On ACF diagrams (Fig. 6), a trend in the data points reflects

Fig. 4. Pillow lavas exposed in the Bosch Aar road cutting. The author is pointing at the rim of a large pillow, and a smaller pillow above it shows a sag structure.

Table 4
Representative pyroxene compositions and structural formulae from the Ongeluk lava

	77391/5	77391/6	77391/7	77391/10	77391/11	77391/18	JU5/14
SiO_2	51.53	48.69	50.98	49.43	49.45	55.76	49.28
TiO_2	0.42	1.39	0.42	0.50	0.53	0.45	0.25
Al_2O_3	4.12	5.26	4.01	2.94	3.32	3.55	3.85
FeO(T)	11.81	15.39	11.41	14.66	12.02	13.29	13.67
MnO	0.27	0.32	0.26	0.28	0.27	0.27	0.46
MgO	16.40	12.68	14.70	13.77	15.21	12.00	11.33
CaO	15.60	16.01	17.84	17.82	18.13	13.19	20.81
Na_2O	0.19	0.54	0.43	0.16	0.14	0.32	0.33
K_2O	0.00	0.00	0.00	0.00	0.00	0.08	0.09
Total	100.33	100.28	100.12	99.57	98.08	98.91	100.07
Si	1.904	1.843	1.900	1.888	1.877	2.063	1.882
Al^{IV}	0.096	0.157	0.100	0.112	0.123	0.000	0.118
Al^{VI}	0.083	0.078	0.076	0.021	0.026	0.155	0.055
Ti	0.012	0.040	0.012	0.014	0.015	0.013	0.007
Fe	0.365	0.487	0.356	0.468	0.382	0.411	0.436
Mg	0.903	0.716	0.817	0.784	0.860	0.662	0.645
Ca	0.617	0.650	0.712	0.729	0.737	0.523	0.851
Na	0.014	0.039	0.031	0.012	0.010	0.023	0.025
Mn	0.008	0.010	0.008	0.009	0.009	0.008	0.015
Ca–Mg–Fe proportions (in %)							
Ca	32.6	34.9	37.6	36.6	35.6	32.6	43.7
Mg	47.7	38.4	43.2	39.4	41.6	41.3	33.1
Fe + Mn	19.7	26.7	19.2	24.0	22.8	26.1	23.2

The structural formulae are based on six oxygens. Oxides are given in wt.%.

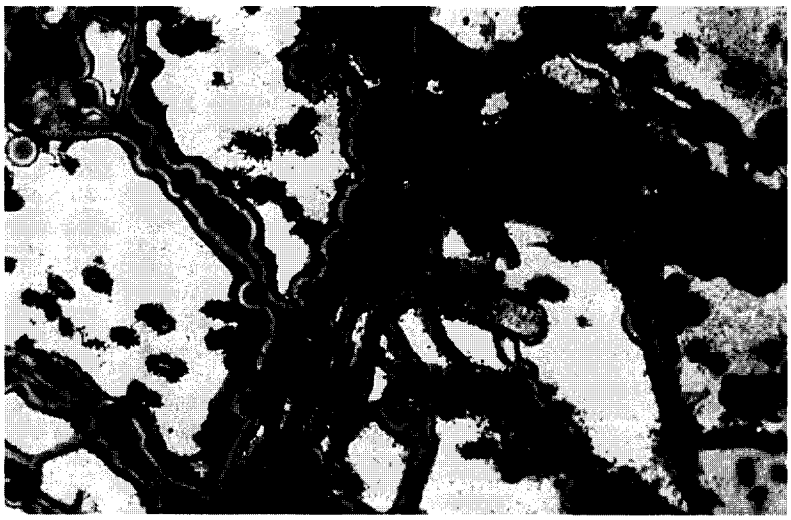

Fig. 5. Photomicrograph of a fragment of hyaloclastite, clear glass fragments are surrounded by a system of veins along which dark devitrification has developed. The field of view is 3 mm.

Table 5
Average chemical analyses with absolute standard deviations for subsets of the Ongeluk and Hekpoort lavas (where sample levels were below detection limits, the analytical value was used in calculations)

	Regional Ongeluk		'Selected' Ongeluk		Western Hekpoort		Boven Ongeluk [a]		Bosch Aar [b]	
	$n = 104$	std.dev.	$n = 38$	std.dev.	$n = 49$	std.dev.	$n = 7$	std.dev.	$n = 4$	std.dev.
SiO_2	56.24	2.77	56.04	1.03	57.07	1.92	55.56	1.08	55.2	0.23
TiO_2	0.65	0.05	0.65	0.03	0.61	0.05	0.66	0.03	0.64	0.01
Al_2O_3	14.32	1.19	14.52	0.39	14.98	1.34	14.55	0.19	14.74	0.15
$Fe_2O_3(T)$	10.65	1.19	10.78	0.5	10.05	0.95	10.89	0.37	10.86	0.37
MnO	0.14	0.02	0.14	0.01	0.15	0.02	0.15	0.01	0.14	0
MgO	5.84	0.95	5.93	0.46	6.4	1.82	5.8	0.16	5.86	0.22
CaO	8.87	3.16	8.79	1.63	8.23	1.6	9.83	0.86	8.82	0.76
Na_2O	2.66	1.42	2.77	0.55	1.83	0.72	2.64	0.85	2.87	0.52
K_2O	0.76	0.84	0.62	0.52	0.8	0.61	0.23	0.13	0.91	0.25
P_2O_5	0.1	0.02	0.1	0.01	0.1	0.02	0.09	0.01	0.1	0.01
V	201.1	14.6	203.4	11.4	177.6	9.8	211.9	3.2	217.0	4.2
Cr	128.4	79.8	126.6	57.3	375.4	229.8	82.7	2.3	85.5	1.5
Ni	84	14.4	85.1	5.7	69	7.6	86.6	3.1	87.8	2.5
Cu	62.2	17.6	61.5	11	117.8	47.3	66.6	9.4	70.5	2.9
Zn	69.9	14.3	73.6	11.2	56.9	96.6	76.6	17	79.5	4.0
Ga	14.6	3.1	14.6	1.9	15.7	1	15.5	0.5		
Rb	34.5	33.5	32.4	24.3	38	29.3	14.1	6.8	36.8	10.2
Sr	164.1	130	210	66.3	143.8	94	195.1	67.1	270.8	18.7
Y	22.5	2.3	22.7	1.4	16.5	3.3	24	0.5	22.8	0.4
Zr	104.2	9.2	104.5	5.1	116.4	17.2	105	1.5	104.5	0.9
Nb	5.8	0.7	5.6	0.7	4.6	1.8	5.9	0.3	5.8	0.4
Ba	256.9	178.1	268.2	169.8	–	–	145.4	39.6	321.3	74.6
Pb	8.5	11.5	7.3	2.2	–	–	5.1	0.6	6.8	1.1
Th	6.8	1.7	6.8	1.4	–	–	5.7	1.5	6.8	1.1
U	1.7	1	1.8	1	–	–	1.4	0.7	1.6	0.8

[a] Successive flows.
[b] Massive lava.

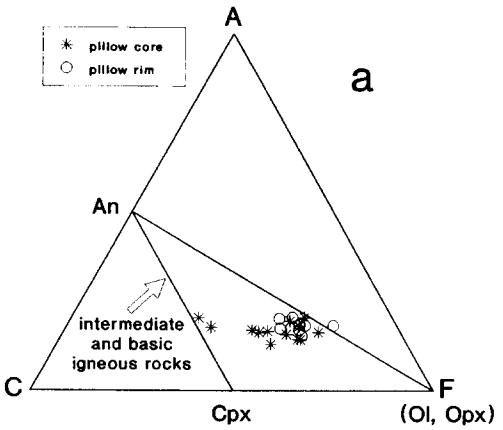

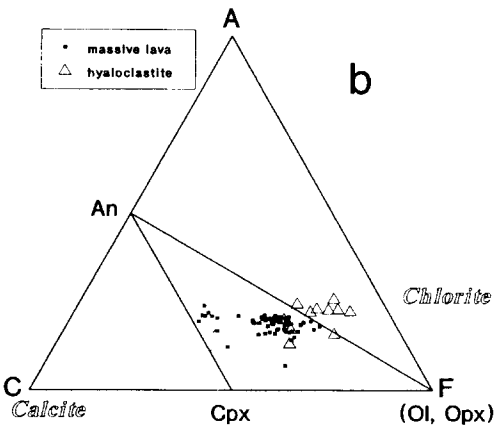

Fig. 6. ACF diagrams showing: (a) Ongeluk pillow cores and rims; (b) Ongeluk massive lava and hyaloclastite samples.

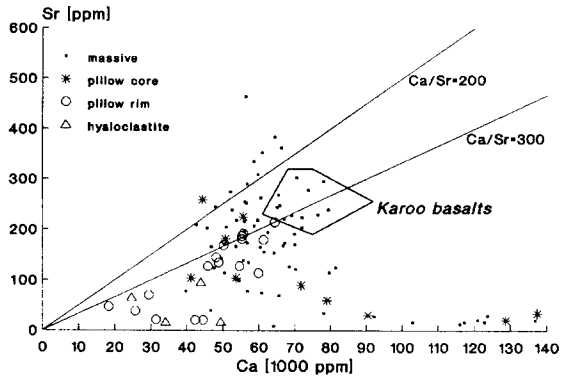

Fig. 7. Ca–Sr plot for Ongeluk lavas, with the field of unaltered Karoo lavas from Marsh (1987), for comparison.

gain and loss of Ca, causing some hyaloclastite samples to plot outside the igneous cpx–opx–plag triangle. Fig. 7 shows a major decoupling of Sr from Ca in many samples. Ca and Sr loss is probably due to leaching from volcanic glass and plagioclase, while Ca gain is related to the precipitation of calcite or epidote from solution in post-magmatic alteration. Similar decoupling is seen on K vs Rb and other plots. Before examining the alteration in detail, an estimate of the original composition of the igneous rocks will be made.

6. Original composition of the Ongeluk lava

Hughes (1973) established a criterion for the recognition of alkali alteration in igneous rocks, whereby samples plotting outside the 'igneous spectrum' shown in Fig. 8 can be regarded as altered. Using this and other alteration criteria summarised in Table 6, a 'selected dataset' of 38 samples was chosen by excluding samples which failed one or

Table 6
Criteria used to create the 'selected dataset'

Criterion for acceptance	Reference or reason	No. samples failed
Plot inside igneous spectrum.		
on alkalis vs. (potash/alkalis)	Hughes (1973)	23
Less than 4.0% LOI	McLean (1991)	14
No normative corundum	peraluminous indicates Ca-loss	6
More than 0.5% Na_2O	less than this suggests Na-loss	1
$Fe_2O_3/(FeO + Fe_2O_3)$ less than 0.5 (where FeO analysis done)	oxidisation suggests alteration	12
mg number less than 47	outliers on histogram (mean 53.5, std.dev. 1.5)	4

more criteria. The mean values and standard deviations for the selected dataset are compared with those for some other datasets in Table 5. The selected dataset has much smaller standard deviations than the total regional dataset, but shows very similar mean values. This suggests that the nett effect of alteration in massive lavas of the regional Ongeluk was a redistribution of elements within the formation. By contrast, studies of the Kalahari Ongeluk to be published elsewhere show that large-scale hydrothermal systems operated there.

6.1. Classification

With only two exceptions (andesite), all samples of the selected dataset plot in the basaltic andesite field of the total alkali–silica diagram, which has been adopted by IUGS (Sabine, 1989) for classification of volcanic rocks. The Ongeluk selected mean analysis has similar low Ti and Mg values to Phanerozoic andesites (e.g. Gill, 1981). The low alumina level of 14.5% compared to 16–20% in Phanerozoic calc-alkaline rocks, causes Ongeluk samples to plot in the tholeiitic rather than the calc-alkaline field of Irvine and Baragar's (1971) alumina vs anorthite plot. In the AFM diagram of Fig. 9 a tholeiitic affinity is also seen.

6.2. Homogeneity

Four Bosch Aar samples from a single lava flow, and seven Bovenongeluk samples from successive

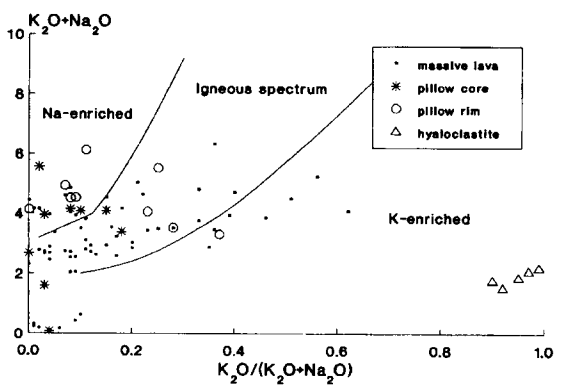

Fig. 8. Hughes' (1973) criterion for alkali alteration applied to Ongeluk samples.

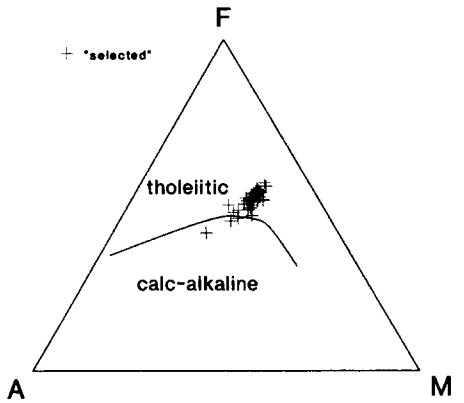

Fig. 9. AFM diagram for the 'selected' Ongeluk dataset shows a tholeiitic affinity.

flows in a 200 m hill section, both show similar mean values and low standard deviations in Table 5. The average analysis of Western Hekpoort samples analysed by Engelbrecht (1986) is indistinguishable from the selected dataset for all elements, which confirms the stratigraphic correlation. The compositional homogeneity, reflected by low standard deviations of the mainly terrestrial Hekpoort lavas, suggests that they are less altered than the submarine Ongeluk lavas.

We interpret the close agreement of all mean values in Table 5 to indicate that the 'selected' mean value closely approximates the original composition of the samples.

6.3. Heterogeneity

To investigate heterogeneity which might be due to igneous processes, various plots were made. The only one which shows significant trends is the Cr vs magnesium number (mg) plot of Fig. 10a. This suggests that the Ongeluk samples conform to two types, distinguished by their Cr levels, which may be related to igneous evolution. Data for the western Hekpoort lavas from Engelbrecht (1986) plotted in Fig. 10b, show that the high-Cr Ongeluk samples plot close to the end of a much longer Hekpoort trend broadly related to stratigraphic height, while the low-Cr Ongeluk type is either absent from or only represented by one sample in the lower Hekpoort. The stratigraphic height of Ongeluk samples is difficult to determine; however, the profile

across the Ongeluk–Witwater syncline shown in Fig. 11 shows that both lower- and uppermost lavas have low Cr, with the high-Cr type occurring just above the base. This pattern is more easily related to contamination or source-heterogeneity than to igneous fractionation. Thus the early and later Ongeluk magmas were a low-Cr type, while the incorporation of Cr-rich, high-Mg material during the early stage of eruption led to the large variations in Cr and mg number.

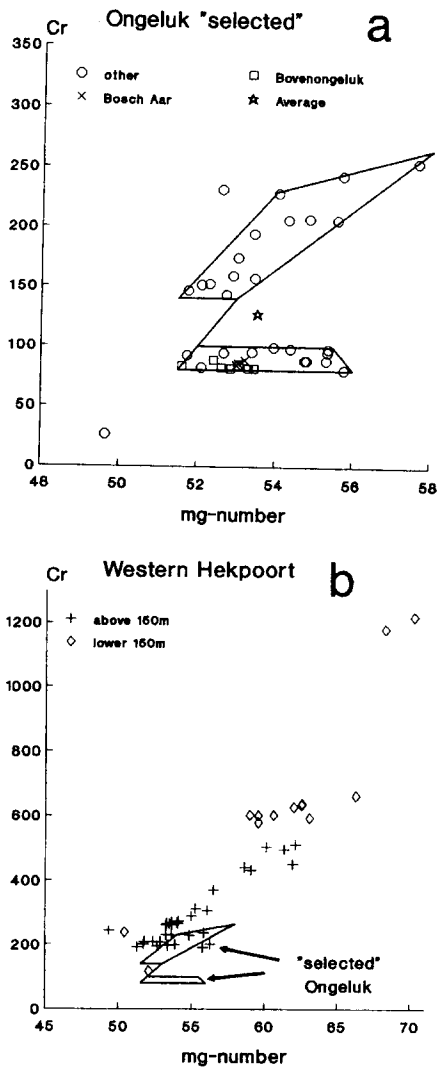

Fig. 10. Cr vs mg number, (a) in the Ongeluk 'selected' dataset, and (b) using a different scale, in samples from the Western Hekpoort correlate. Data from Engelbrecht (1986).

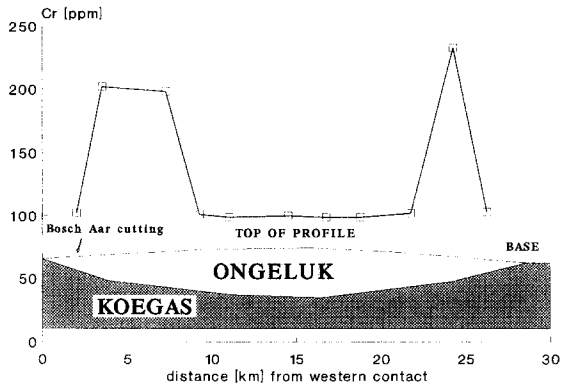

Fig. 11. Cr levels plotted for a profile in the Ongeluk–Witwater syncline shown in Fig. 2, with a schematic geological section. Data from Engelbrecht (1986).

From the above we conclude that the composition of the Ongeluk magma is well approximated by the mean composition and about two standard deviations of the selected dataset, although it was demonstrably heterogeneous within these limits. The alteration of Ongeluk samples may thus be investigated by comparison with the selected dataset.

7. Alteration

An alteration diagram was developed to illustrate the diversity of alteration by normalising each element to the selected average, using a sequence of elements which gives fairly smooth profiles. Fig. 12a shows profiles for a pillow core–rim pair. They depart significantly from mirror images, which suggests that the core and rim exchanged material with a fluid rather than with each other.

The Ongeluk alteration has many macroscopic (e.g. dark chilled pillow rims, hyaloclastites) and microscopic (e.g. palagonitization) features in common with ocean-floor spilitic alteration. Because the changes in composition are not developed on a large, pervasive scale, but rather related to the small-scale changes from pillow core to rim, or flow centre to margin, the Ongeluk lavas are thought to have been altered by interaction with the water under which they formed. A literature review of modern seafloor alteration revealed a great diversity of products and processes, some of which are outlined below, illus-

trated by alteration diagrams normalised to the unaltered composition in each case.

7.1. Modern seafloor alteration

The alteration of modern seafloor basalt is controlled by four main variables: temperature, depth (controls boiling temperature), water/rock ratio and position in hydrothermal system (inflow or exhalation). According to Thompson et al. (1983) the most common types of seafloor alteration are: (1) low-temperature high water/rock ratio, found near the water–rock interface; (2) low-temperature low water/rock ratio, due to long-term circulation of cool seawater into the crust; and (3) high-temperature (> 100°C) alteration driven by magmatic heat near

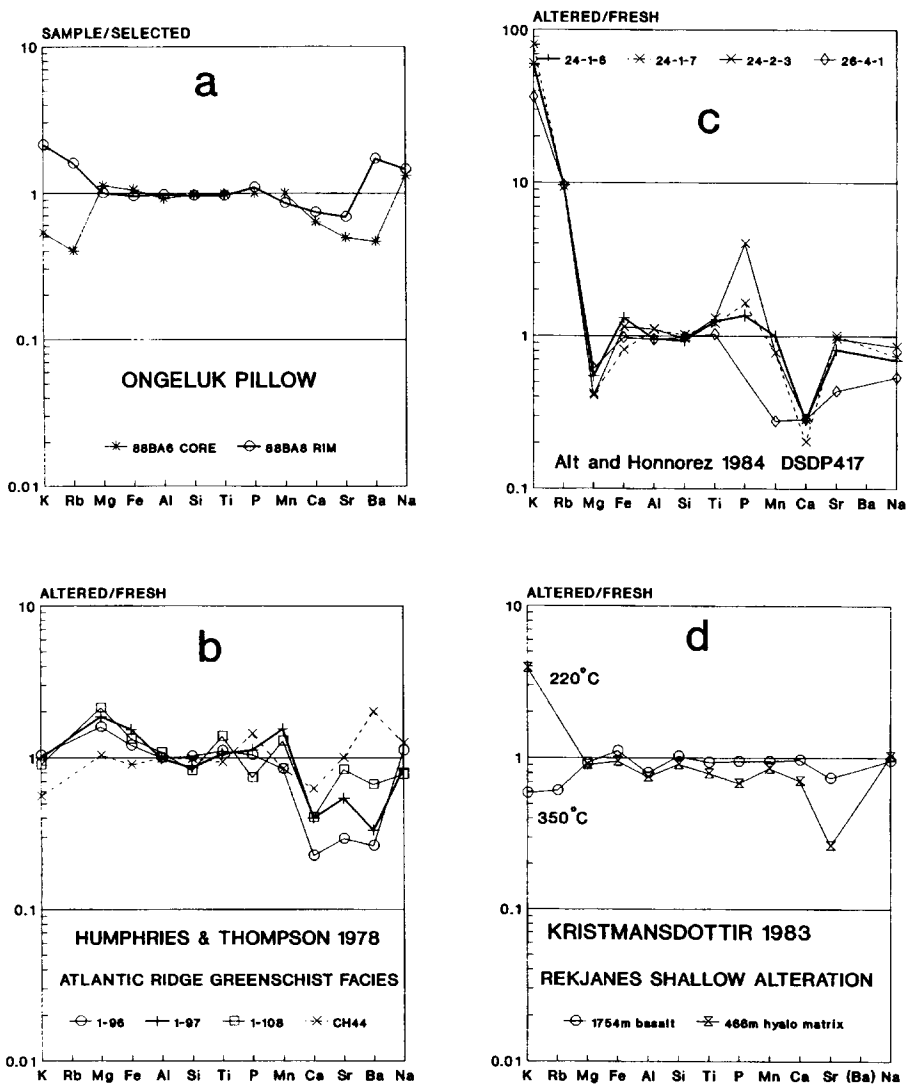

Fig. 12. Alteration diagrams developed to illustrate the effects of seawater alteration. (a) An Ongeluk pillow core–rim pair. (b) Greenschist-facies-altered basalt from the mid-Atlantic ridge; data from Humphris and Thompson (1978). (c) Deep Sea Drilling Project Atlantic Ocean site 417; samples from Bermuda Rise, from Alt and Honnorez (1984). (d) Rekjanes, Iceland samples showing shallow-seawater alteration, described by Kristmansdottir (1983).

spreading centres. Cann (1979) proposed submarine alteration facies named brownstone, zeolite, greenschist and amphibolite in increasing order of temperature. Judging from the minerals identified in the fine-grained Ongeluk samples and the chlorite geothermometry (227–264°C), Ongeluk alteration corresponds to the first two or three facies.

7.2. Deep-sea alteration

Greenschist-facies pillow basalt from the Mid-Atlantic Ridge analysed by Humphris and Thompson (1978) are featured in Fig. 12b. These represent Thompson et al.'s (1983) high-temperature alteration. The notable features are enrichment of Mg and Fe, probably concentrated in chlorite, and depletion (from plagioclase?) of Ca, Sr and Ba with variable behaviour of Na related to changes in the stability of albite. Alteration profiles for samples from DSDP site 417, analysed by Alt and Honnorez (1984) are shown in Fig. 12c. These represent low-temperature (> 50°C) high water/rock ratio alteration of basalt, possibly in the discharge site of a convection system. The major enrichment of K and Rb which these

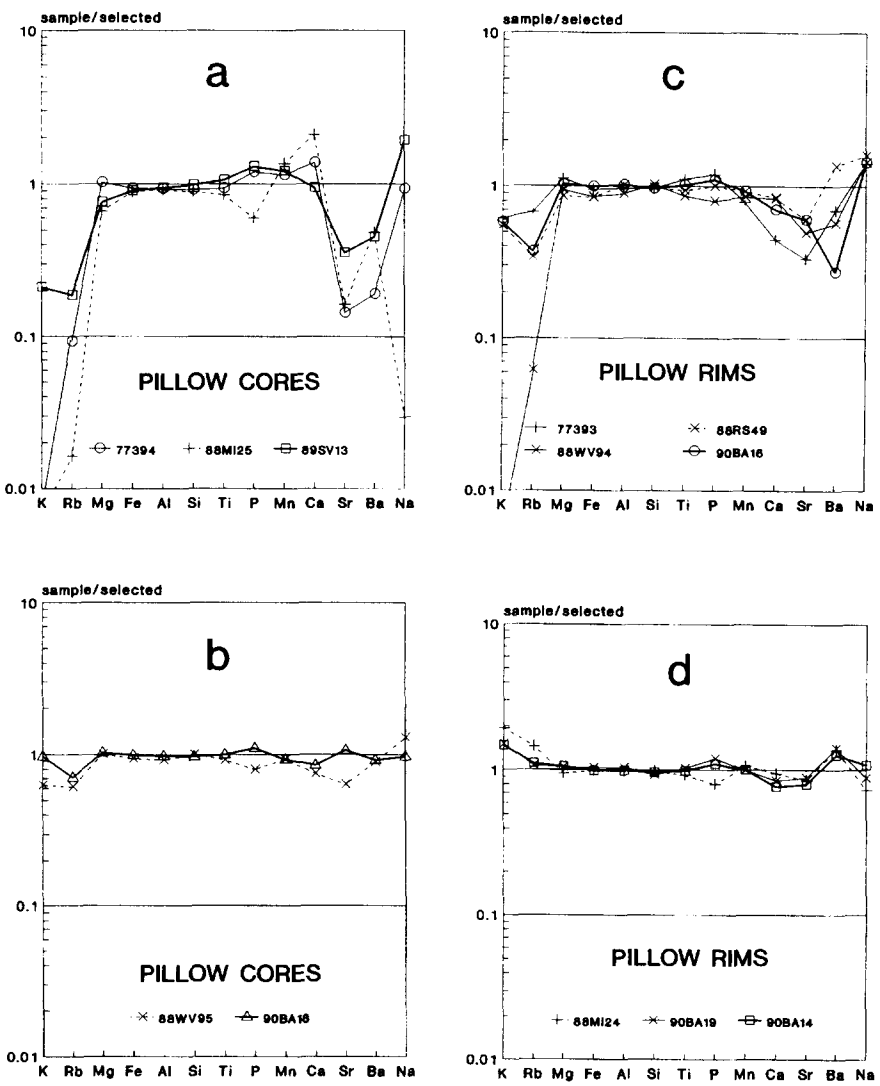

Fig. 13. Alteration diagrams for: (a) and (b), Ongeluk pillow cores; (c) and (d), pillow rims.

samples show is related to the formation of clay minerals and K-feldspar, while Ca and Mg are lost to the low-temperature fluid due to the instability of both Ca-feldspar and Mg-silicates such as pyroxene or chlorite.

7.3. Shallow-marine alteration

The Reykjanes geothermal field of Iceland, described by Kristmansdottir (1983) might be analogous to the shallow-marine Ongeluk alteration, because its seawater–rock interaction occurs close to the surface, at much lower pressures than for ocean-floor samples. Alteration diagrams constructed for 17 borehole samples of basalt, hyaloclastite and tuff from this site, show rather variable patterns, two of which are shown in Fig. 12d. The K-enrichment, shown by a sample altered at 220°C, changes to K-depletion at a higher temperature of about 350°C. Decoupling of Ca and Sr is also apparent, Sr being severely depleted in the 220°C hyaloclastite.

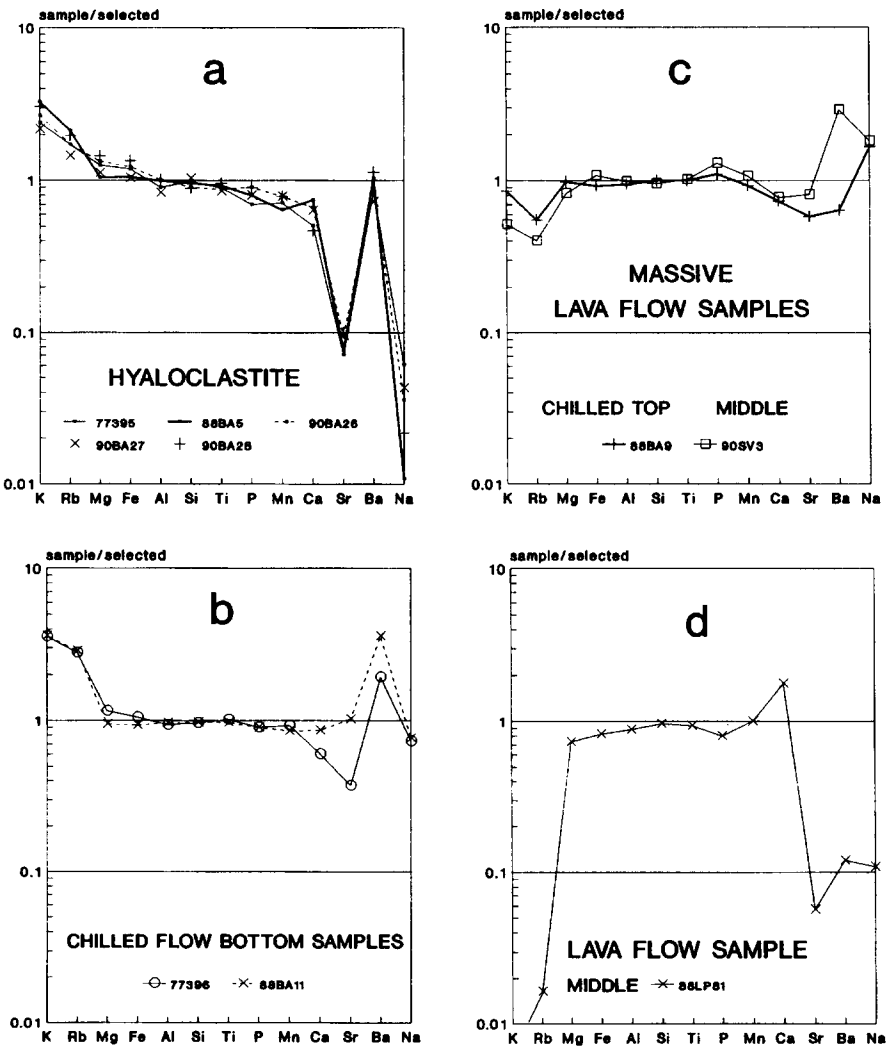

Fig. 14. Alteration diagrams for: (a) Ongeluk hyaloclastites; (b), (c), (d), lava flow samples.

8. Alteration of Ongeluk pillows and hyaloclastites

To avoid long descriptions of the diversity and complexity of Ongeluk alteration, the geochemical data for pillows and hyaloclastites is described in relation to an alteration model which accounts for most of the field, petrographic and geochemical data. The data for lava flow samples is then discussed in relation to the model. Finally, isotope data for all sample types is reported.

The interaction of pillow lavas and hyaloclastites with water is visualised in terms of three temperature-related alteration classes. Class 1 interaction is prevented in this shallow-marine case by a sheath of steam surrounding the rapidly cooling pillows or lava fragments. At great depths of > 2300 m, steam would not form, permitting very high temperature class 1 interaction; however, this possibility is excluded by the presence of amygdales in the Ongeluk. Once the lava cools below boiling point (depending on the water depth), water enters via cracks and class 2, relatively high-temperature alteration proceeds, enhanced by the convective circulation of the water.

After the lava cools to the same temperature as the surrounding water, convective circulation drops off and a long period of class 3 'low-temperature' alteration begins. Pillow cores are likely to show mainly class 2 effects, as they would remain hot longer than the rims, and are accessed by deep cracks in pillows. Rims should show a combination of class 2 and 3 effects, as they present a large surface area during both stages. Hyaloclastites with much smaller fragments should cool rapidly and exhibit major class 3 alteration due to the high permeability of hyaloclastite beds.

8.1. Class 2 alteration

Pillow cores as examples of class 2 alteration commonly show severe depletion of K and Rb as shown in Figs. 13a and 13b. This suggests that micas did not form during class 2 alteration. Sr and Ba are generally also depleted, while Ca and Na are variable, suggesting changes in feldspar stability due to variations in temperature and water/rock ratio. At near-surface pressures calcic plagioclase breaks down at temperatures around 350°C, while according to Jasinski et al. (1985), albite is not stable below 150°C. Both the K and Rb depletion and decoupling of Ca and Sr are analogous to the Rekjanes 'shallow' (1750 m) 350°C process, while the 220°C Rekjanes sample shows K-enrichment. This suggests that class 2 began at temperatures between 250° and 350°C, requiring water depths between 400 m and 1680 m, respectively.

8.2. Class 3 alteration

Hyaloclastites exhibit rather constant alteration profiles in Fig. 14a, suggesting that equilibrium might have been attained between water and hyaloclastite. This class 3 alteration increased K, Rb, Mg and Fe, probably due to the development of micas and chlorite. A small but general depletion of Mn suggests a reducing alteration environment removing Mn^{2+}, while the increasingly severe depletion of Ca, Sr and Na suggests the instability of both calcic plagioclase and albite during this stage. The relatively unaltered Ba level might be related to barite formation, sulphate being provided by the water in a water-dominated system. The enrichment of K and Rb at temperatures below 220°C is confirmed by both Rekjanes and DSDP data while Sr depletion decoupled from Ca is shown only by the former and Na depletion by the latter, and Ba data is lacking in both cases.

No literature examples were found of sodium depletion on the scale shown by Ongeluk hyaloclastites; however, Mottl (1983) ascribed less dramatic Na losses from basalt to high (> 10) water/rock ratios. He also found experimentally that in seawater alteration Ca loss was closely balanced by Mg gain, a feature shown by the Ongeluk hyaloclastite in Fig. 15.

The hyaloclastite data is thus consistent with class 3 alteration having established equilibrium with water between about 200° and 50°C. The water would probably have been trapped within the volcanic pile, thus maintaining an elevated temperature for sufficiently long to equilibrate with the hyaloclastite fragments.

The pillow rim alteration profiles in Figs. 13c and 13d generally show less severe alteration than cores. The more altered samples show class 2 features like the cores, while the less altered ones have more in

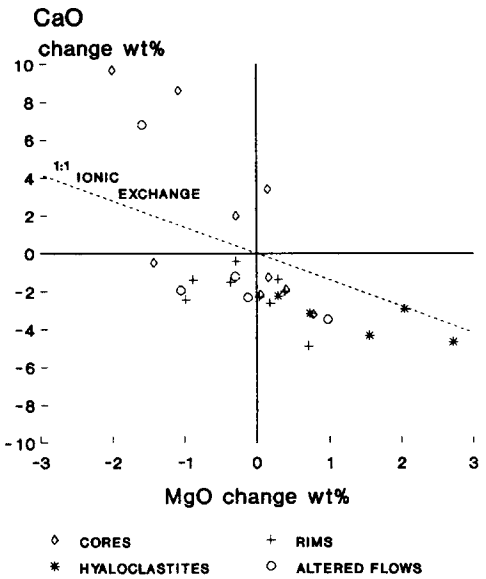

Fig. 15. The relationship between Ca and Mg alteration relative to the original magma composition is shown for the different Ongeluk rock types.

common with class 3 hyaloclastites. The diversity of their profiles can thus be accounted for in terms of combinations of class 2 and 3 processes.

8.3. Massive lava flow alteration

Massive lava flow sample alteration diagrams in Figs. 14b and 14d show different characteristics depending on their positions in the flow. Two chilled flow bottom samples in Fig. 14b have profiles like those of hyaloclastite, suggesting predominant class 3 alteration. One chilled flow top sample and a mid-flow sample in Fig. 14c show alteration diagrams like those of pillow cores, reflecting class 2 alteration, while another mid-flow sample (Fig. 14c) represents an extreme of class 2. It is suggested that the hot flow bottoms expelled all water from their vicinity before the flow cooled to boiling point. The flow bottoms thus escaped class 2 alteration, which only affected the flow top and mid-flow regions as water penetrated cracks from above. Later slow ingress of water along the flow bottom plane led to low-temperature class 3 alteration of the pristine igneous rock.

8.4. Validity of the model

Although the seawater alteration model described above cannot be proven correct, it does account for most of the geochemical alteration features observed, and is consistent with geological evidence as to textures and rock types, and with literature data. Although post-depositional alteration by formation waters or hydrothermal solutions might well have affected some of the samples, it would be difficult to explain the diversity of alteration by a diagenetic or hydrothermal process, which should give rise to pervasive alteration at a fairly constant temperature. The different alteration trends of pillow cores and rims would in particular favour the seawater alteration model.

9. Rb–Sr data

9.1. Previous Ongeluk and Hekpoort data

Crampton, reported in Hamilton (1977), gave a date of 2224 ± 21 Ma (R_0 0.7082) for four Hekpoort lava samples from Western Deep Levels near Rustenburg, combined with one Smelterskop lava sample. These samples were collected by A. Button and analyzed in 1973 by D. Crampton at the Bernard Price Institute for Geophysical Research, University of the Witwatersrand. These previously unpublished data were provided by the late H. Allsopp, (pers.

Table 7
Rb–Sr data for Hekpoort lavas, analysed by D. Crampton at the Bernard Price Institute, University of the Witwatersrand (H. Allsopp, pers. commun., 1977), and previously unpublished

Sample	Depth (m)	Rb (ppm)	Sr (ppm)	$^{87}Rb/^{86}Sr$	$^{87}Sr/^{86}Sr$
OL/K4/42	502	63.15	88.18	2.081	0.7734
OL/K4/45	800	82.73	404.1	0.5923	0.7263
OL/K4/46	782	170.2	142.0	3.500	0.8181
OL/K4/48	739	99.34	88.44	3.276	0.8105
FJC 13	131.3	198.4	28.91	1.4437	
Est. uncertainty				2%	0.0004

The OL/K4 samples are massive or amygdaloidal andesites from borehole K4 on Kalbasfontein 365, lat. 26°30′S, long. 27°40′E, and concentrations are by isotope dilution. FJC 13 is an andesite sample from the 'Smelterskop' in the Rooiberg area, concentrations by XRF, but $^{87}Rb/^{86}Sr$ ratio by ID.

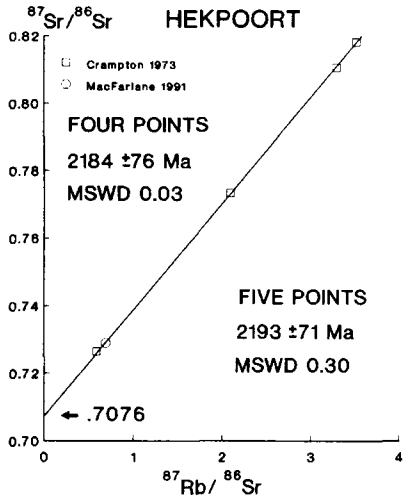

Fig. 16. Rb/Sr isochron diagram showing four Hekpoort lava samples from Western Deep Levels near Rustenburg analyzed by D. Crampton and one 'unaltered' Hekpoort palaeosol profile sample analyzed by MacFarlane and Holland (1991).

commun. to D.H.C. 1977), and are given in Table 7. Recalculation of these four data with GEODATE (Eglington and Harmer, 1991) and the new decay constant (Steiger and Jäger, 1977), excluding the Smelterskop sample which is stratigraphically younger, results in an isochron date of 2184 ± 76 Ma (MSWD: 0.027; R_0 0.7076 ± 0.0008). Inclusion of one 'unaltered' sample from a Hekpoort palaeosol profile (85-ZH-20) analyzed by MacFarlane and Holland (1991) results in a slightly older date (2193 ± 71 Ma) with higher MSWD (0.302 on 5 points) and lower initial ratio (R_0 0.7071) as shown in Fig. 16. Armstrong (1987) determined a nine-point errorchron date of 2023 ± 217 Ma for Bosch Aar Ongeluk samples, with high MSWD = 17.7 and initial ratio of 0.7069. He ascribed the errorchron scatter to open system behaviour, clearly related to the seafloor alteration described in this work. Because the Hekpoort is considered to be subaerial and much less altered than its Ongeluk correlate, the 2184 Hekpoort isochron is considered to provide a better estimate of the age and initial ratio of the Hekpoort and Ongeluk lavas.

9.2. Alteration of Sr isotopes

Fig. 17a shows an isochron diagram for regional Ongeluk samples, corrected to 2184 Ma, with the Hekpoort isochron for comparison, as it should represent an unaltered equivalent of the Ongeluk (data in Table 8). Focusing on the low Rb/Sr samples in Fig. 17b, most samples have lower initial ratios than the Hekpoort isochron, while four pillow core and massive lava samples lie above it. A simple model for seafloor alteration of lava with higher initial ratio by seawater with lower Sr initial ratio could explain much of the data; however, those samples with high initial ratios cannot be accounted for by this model. A geochemical criterion, which identifies those anomalous samples for which Ca concentrations are available, is shown in Fig. 18. The anomalous samples, including the three hyaloclastites, all have

Table 8
Rb–Sr data for Ongeluk lava samples analysed for this work

Sample	Rock type	Rb (ppm)	Sr (ppm)	$^{87}Sr/^{86}Sr$	$^{87}Sr/^{86}Sr$	$^{87}Sr/^{86}Sr_i$
77393	rim	20.74	68.69	0.8756	0.73177	0.70408
77394	core	1.337	37.20	0.1041	0.71429	0.71099
77395	hyalo	50.47	22.19	6.727	0.93469	0.72191
77397	massive	31.97	164.60	0.5629	0.72404	0.70623
88BA5	hyalo	74.24	22.20	9.953	1.00103	0.68621
88BA6	core	11.81	99.98	0.342	0.71770	0.70688
88BA8	rim	47.87	135.02	1.028	0.73453	0.70199
90BA18	core	24.65	235.99	0.302	0.71571	0.70614
90BA19	rim	37.10	185.90	0.578	0.72115	0.70287
90BA20	outer core	6.454	97.00	0.1926	0.71540	0.70930
90BA28	hyalo	68.80	28.37	7.177	0.94164	0.71463
Analytical precision					0.8%	0.00014

Concentrations are by isotope dilution. Sr_i initial ratios are calculated for 2184 Ma.

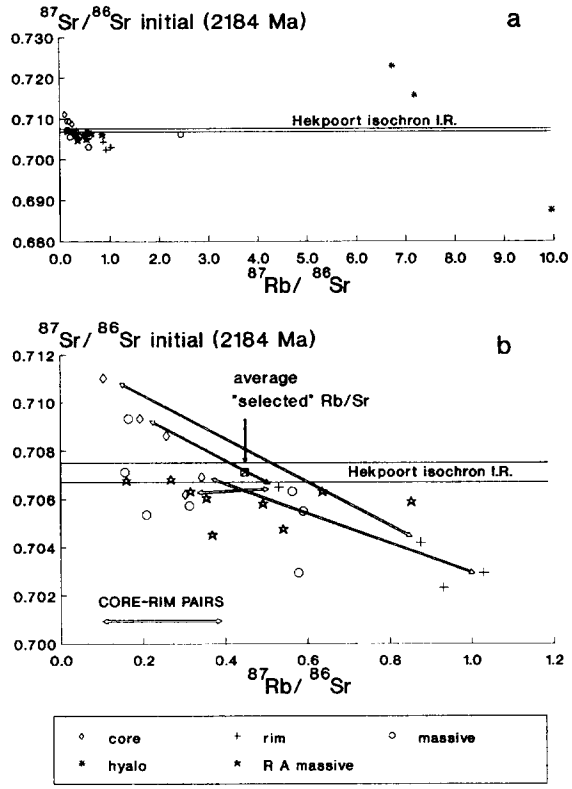

Fig. 17 Initial ratio diagrams: (a) for all regional Ongeluk samples, corrected to 2184 Ma, with the Hekpoort isochron for comparison; (b) omitting the high Rb/Sr samples.

Ca/Sr above 500, due mainly to low Sr levels (20–100 ppm), hence they were highly susceptible to Sr alteration.

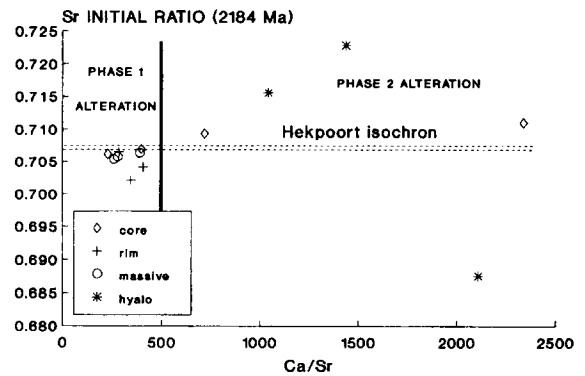

Fig. 18. Ca/Sr vs Sr initial ratio shows that only samples with Ca/Sr above 500 depart from a single-phase seawater alteration model.

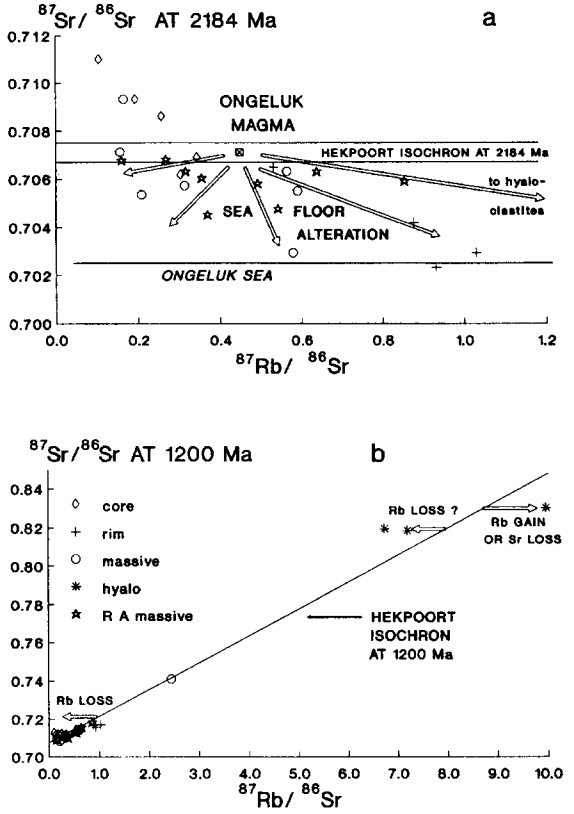

Fig. 19. Two-stage model to explain the alteration of Sr isotope ratios. (a) At the time of origin interaction with seawater lowers initial Sr isotope ratios of some samples towards 0.7025. (b) At 1200 Ma low-Sr samples are moved horizontally away from the (then 984 Ma) isochron line during the introduction of calcite.

9.3. Two-phase alteration model

A two-phase alteration model is needed to account for the Sr isotope data as illustrated in Fig. 19. In phase 1 at the time of extrusion, the Ongeluk lava with $^{87}Sr/^{86}Sr = 0.7071 \pm 8$ (the same as Hekpoort), undergoes (classes 1 and 2) interaction with the $^{87}Sr/^{86}Sr \sim 0.7025$ Ongeluk sea, thus lowering the initial ratio of most samples as shown in Fig. 19a.

The sketchy data on Proterozoic marine Sr isotopes, summarised by Faure (1986), suggest marine $^{87}Sr/^{86}Sr$ between 0.702 and 0.704 at 2.2 Ga. Veizer et al.'s (1989) 'best estimate' of 0.70550 for Malmani and other Palaeoproterozoic dolomites is regarded as an imprecise upper limit, in view of the large scatter of data (0.705 to 0.750) in samples

described as diagenetically altered. Furthermore, Turner (1992) obtained initial ratios as low as 0.7022 for carbonate rocks from Pering lead mine in the Malmani equivalent of Griqualand West.

Phase 2 of the two-phase alteration model takes place long after the volcanic genesis of the formation, by which time the array of sample data points has developed a slope on the isochron diagram shown in Fig. 19b. At this time circulating fluids introduce calcite or epidote, increasing Ca/Sr and significantly changing the Rb/Sr ratio of low-Ca samples, causing them to move horizontally on the diagram. Most of the affected samples suffer Rb loss or gain Sr, moving above the Hekpoort isochron. However, the hyaloclastite sample 88BA5 must have lost Rb or gained unradiogenic Sr long after extrusion, to explain its impossibly low present-day initial ratio of 0.686, and this sample cannot be accounted for by any multi-component process at the time of extrusion. The second phase of alteration, taking place long after extrusion, would be restricted to fractures in massive and pillow lavas, but would be more general in porous rocks like hyaloclastite.

9.4. Age of second phase

Although the Ongeluk lava shows little sign of regional metamorphism, its situation at the tectonic boundary between the Kheis Province and Kaapvaal Craton suggests that it could have been influenced by tectonic events in the Kheis foreland. The age of the Kheis tectogenesis is probably between 1928 Ma and 1750 Ma (Cornell et al., 1996); however, there is little evidence for fluid movement in the Kheis foreland at this time. A more probable time for the second phase of alteration is the 1257 ± 11 Ma Rb/Sr date reported for an Ongeluk 'palaeosol' by MacFarlane and Holland (1991). This clearly reflects an episode of fluid movement and corresponds to some other dates from the Kheis Province foreland: 1004 Ma Rb/Sr and 1100 Ma K/Ar from Okwa, Botswana by Key and Rundle (1981) and 1270 to 1350 Ma Pb–Pb model and errorchron ages from Kalahari Mn mines by Dixon (1989). It coincides with the 1210 Ma first collision of the Namaqua–Natal tectogenesis south of Prieska (Cornell et al., 1992), which also reset K/Ar in clay minerals on the Kaapvaal Craton (U.E. Horstmann, pers. commun., 1992). The extent to which the Kheis Province was affected by the Namaqua tectogenesis is poorly understood.

9.5. Numerical modelling of phase 1 Sr-isotopic changes

Numerical modelling of Sr and Sr-isotope (for samples with initial ratios below 0.7071) alteration by water–rock interaction was attempted. It was not possible to simulate the alteration by varying only one parameter. The low-Sr class 3 altered samples require low rock/water partition coefficients around 2.5, with water/rock ratios between 80 and 200. The class 2 and class 3 altered pillow rim samples require higher partition coefficients between 6 and 20 and water/rock ratios between 1 and 200, while several class 2 massive lava and core samples which gained Sr need very high partition coefficients. A maximum water/rock ratio of 200 which is applied to Pb-isotope alteration below, was the only useful result of this exercise.

10. Pb isotope data

10.1. Previous work

Armstrong (1987) reported a 2239^{+68}_{-72} Ma Pb–Pb isochron for nine Bosch Aar lavas. His U/Pb data show evidence of recent U loss. Using GEODATE v. 2.2 (Eglington and Harmer, 1991) a 2236^{+38}_{-39} Ma errorchron shown in Fig. 20 (MSWD = 5.3, μ_2 = 11.87) is obtained, due to a more sophisticated treat-

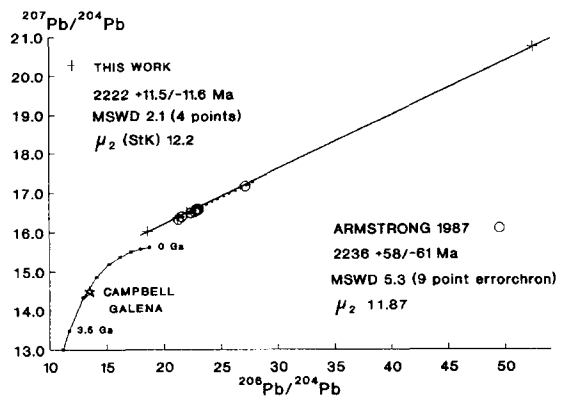

Fig. 20. Pb–Pb isochron diagrams showing the errorchron of Armstrong (1987) (dashed) and the isochron of this work, with the Stacey and Kramers (1975) second-stage evolution curve and a Campellrand galena analysed by Turner (1992).

Table 9
Pb isotope analyses of Ongeluk lava

Sample	$^{206}Pb/^{204}Pb$	$^{207}Pb/^{204}Pb$	$^{208}Pb/^{204}Pb$	$^{207}Pb/^{206}Pb$	$^{208}Pb/^{206}Pb$
77393	52.446	20.744	68.020	0.3955	1.2970
77394	22.030	16.505	41.159	0.7492	1.8683
77395	18.587	16.029	37.892	0.8624	2.0386
77397	21.233	16.365	40.494	0.7707	1.9071
Uncertainty	0.09%	0.09%	0.15%		

The error correlation between $^{206}Pb/^{204}Pb$ and $^{207}Pb/^{204}Pb$ is 0.91.

ment of errors and highlighting the difficulty of distinguishing isochrons from errorchrons. Two Hekpoort samples analysed by Armstrong (1987) lie within experimental error of this line, supporting the Hekpoort–Ongeluk correlation and suggesting that Pb-isotope ratios of Ongeluk samples were not dramatically altered in their subaqueous setting.

10.2. New data on altered samples

Four new samples from the Bosch Aar road cutting were analyzed to better evaluate the effects of alteration: a pillow pair, hyaloclastite and massive lava, data for which are given in Table 9. These samples surprisingly yield a 2222 ± 12 Ma Pb–Pb isochron (MSWD 2.1, $\mu_2 = 12.23$), the small age uncertainty being due to the highly radiogenic pillow rim sample shown in Fig. 20. Adding these four samples to Armstrong's dataset yields an unchanged errorchron date of 2237 ± 10 Ma with higher MSWD = 9.47. The slightly higher $^{207}Pb/^{204}Pb$ values of our samples apparent in Fig. 20 might reflect a small interlaboratory bias.

These results suggest that although seawater alteration changed the U–Pb ratios of Ongeluk samples, it hardly affected the Pb isotope ratios. In modern seafloor alteration both Pb loss (Brevart et al., 1981; Vidal and Clauer, 1981) and U enrichment (Michard and Albarede, 1986) have been documented. Assuming relative abundances in the Ongeluk sea of 0.00003 ppm Pb and 8 ppm Sr (modern seawater, Henderson, 1982), compared with Ongeluk lava levels of about 7 ppm Pb and 210 ppm Sr, it is clear that alteration would affect Pb far less than Sr. The possible effects of seawater alteration were calculated using worst-case parameters derived from the Sr isotope modelling. Using water/rock ratios of 200, very high (10^6) partition coefficients, and water $^{207}Pb/^{204}Pb$ ratios one integer less than that of each sample (based on Galena data from the Campbell Dolomite, Turner, 1992), yields $^{207}Pb/^{204}Pb$ decreases of < 0.003, which could change the isochron age by only 0.5 Ma.

10.3. Refined ages for the Ongeluk

Despite the recognised alteration of the analysed samples, it is concluded that both Pb–Pb dates of 2236 ± 60 Ma (Armstrong 1987) and 2222 ± 12 Ma (this work, 1 Ma added to error) represent reliable progressive refinements of the 2184 Ma Rb/Sr Hekpoort age.

11. Sm–Nd data

Sm–Nd data for four samples is given in Table 10. The pillow core, rim and hyaloclastite samples all have significantly lower amounts of Nd and Sm relative to the massive lava sample 77397, with higher Sm/Nd ratios. The data are not sufficiently precise to show evidence of Nd isotopic changes due to alteration, and yield an imprecise 2360 ± 568 Ma isochron (MSWD 1.0, I.R. 0.50969 ± 23), due to the

Table 10
Samarium–neodymium isotope data for Ongeluk lava samples

Sample	Sm	Nd	Sm/Nd	$^{147}Sm/^{144}Nd$	$^{143}Nd/^{144}Nd$
77393	3.316	14.46	0.229	0.1386	0.511855 ± 12
77394	3.390	16.89	0.201	0.1213	0.511539 ± 14
77395	2.975	15.38	0.193	0.1169	0.511525 ± 11
77397	3.666	18.91	0.194	0.1172	0.511532 ± 17

The analytical uncertainty for $^{147}Sm/^{144}Nd$ is 0.6%, for $^{143}Nd/^{144}Nd = 0.006\%$.

small spread of Sm/Nd. ϵ_{Nd} values for 2222 Ma average 0.87 with 95% uncertainty of 0.67, suggesting a slightly depleted mantle source.

12. Discussion

12.1. Geotectonic position of the Ongeluk lava

Various diagrams have been developed for the geochemical identification of tectonic setting, based on modern basaltic rocks. Table 11 summarises the interpretation for Ongeluk lavas derived from these. Seven of them favour an arc-related or calc-alkaline origin, while three suggest a within-plate setting. The spidergram in Fig. 21 shows that the Ongeluk selected dataset has high MORB-normalised values for K, Rb, Ba, Th and Ce, which Pearce (1983) ascribed to a subduction component in rocks like the New Hebrides basalt, shown for comparison. However, the Ongeluk has anomalously low Sr, P and Ti values. The Ongeluk and Hekpoort lavas, extruded onto a large portion of the 900 × 600 km Archaean Kaapvaal Craton, show no geological evidence for subduction, such as chemical zonation away from a volcanic front or structural evidence of continental collision following closure of an ocean basin. The Ongeluk–Hekpoort volcanism corresponds rather to 'within-plate' volcanism, related to extensional basin development on the Kaapvaal craton. As pointed out

Table 11
Comparison of tectonic classifications of Ongeluk lava according to various geochemical criteria

Author(s)	Elements	Tectonic environment
Holm (1985)	TiO_2–Th–Nb/3	WPB
Meschede (1986)	Zr/4–Nbx2–Y	VAB
Mullen (1983)	TiO_2–MnO–P_2O_5	IAT
Pearce (1975)	Cr–Zr	IAB
Pearce and Cann (1973)	Ti–Zr–Y	CA
	Ti–Zr–Sr	CA
Pearce et al. (1975)	TiO_2–K_2O–P_2O_5	WPB
Pearce et al. (1977)	FeO–MgO–Al_2O_3	WPB
Shervais (1982)	Ti–V	IAB
Wood (1980)	Th–Hf/3–Ta	VAB

CA = calc-alkaline basalt; IAB = island arc basalt; OFB = ocean-floor basalt; VAB = volcanic arc basalt; WPB = within-plate basalt.

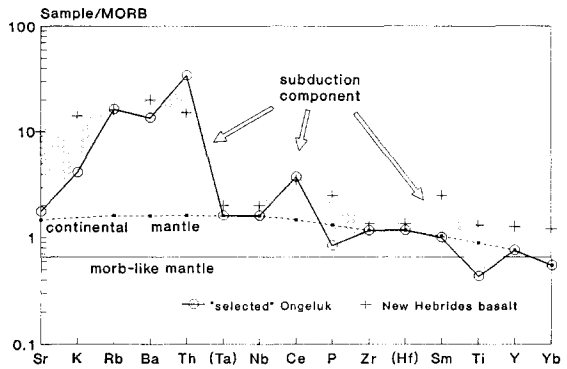

Fig. 21. A MORB-normalised spidergram after Pearce (1983), shows that the Ongeluk selected dataset has high values for K, Rb, Ba, Th and Ce. Mantle and 'subduction' components are identified according to Pearce (1983), compared with the subduction signature of his New Hebrides basalt, discrepancies shaded.

by Harmer and von Gruenewald (1991), the Ongeluk spidergram with its 'subduction' features is typical of most Archaean and Proterozoic basic volcanic rocks of the Kaapvaal Craton, for which no geological confirmation of subduction exists.

12.2. Source of the Ongeluk lavas

Initial isotope characteristics of the Ongeluk–Hekpoort magma are compared with some other mafic rocks from the Kaapvaal Craton in Table 12. The Sr data suggest sources enriched in Rb relative to the UR mantle model for all these magmas. By contrast, the Nd data suggests both light-REE enriched and depleted sources relative to the CHUR model, the Ongeluk having a slightly depleted source. The μ_2 data show that source U/Pb ratios varied

Table 12
Comparison of Ongeluk Formation and some other Kaapvaal mafic rocks in terms of their source isotopic characteristics

	Date (Ma)	ϵ_{Sr}	ϵ_{Nd}	μ_2
Ongeluk and Hekpoort	2222	68	0.9	12.2
Bushveld Mafic unit	2050	48–72	7.0	8.6–11
Hartley Fn basalt	1928	32	−2.9	8.5
Hartley Fn porphyry	1928	5–50	−1.9	8.5
Mantle (UR, CHUR and StK)		0	0	9.7

ϵ_{Sr} and ϵ_{ND} are calculated using UR and CHUR following DePaolo and Wasserburg (1984) and μ_2 according to the two-stage evolution model of Stacey and Kramers (1975). Data from Armstrong (1987), Auret et al. (1990), Cornell et al. (1996).

considerably, the Bushveld magmas having tapped a range of sources during its development, and the Ongeluk being derived from an unusually high-μ_2, U-enriched source. The Ongeluk lavas could be interpreted as a melt derived from an originally depleted mantle source which had been enriched by metasomatism at (say) 3000 Ma, resulting in different signatures related to the different decay constants of ^{87}Rb, U, and ^{147}Sm, respectively. The Kaapvaal isotope data taken together show that the sub-Kaapvaal mantle contains at least two components with different histories of depletion and enrichment.

12.3. The Ongeluk as a source and sink of elements in ocean water

The alteration diagrams discussed above show that several elements were exchanged with the Ongeluk sea in different amounts during the course of alteration. Pillow cores and rims exhibit the most profound losses of alkalis and alkaline earth elements in class 2 high-temperature alteration. However, the low-temperature class 3 alteration typified by the porous hyaloclastite probably had the largest net influence on the Ongeluk sea chemical budget, because of the greater mass of altered material (all the hyaloclastites plus accessible parts of the other rock types), and the long duration of low-temperature alteration. The Ongeluk sea gained most of the Na and Sr contained in the hyaloclastites and significant amounts of Ca and Mn. These exchanges increased the Na/K ratio of the Ongeluk sea and as will be discussed in a later paper, could also represent a significant source of the Mn and Ca contained in the stratiform Kalahari manganese ores which overlie the Ongeluk Lava. The sea lost significant amounts of K, Rb, Mg and Fe to hyaloclastite, although a smaller portion of these elements would have been gained during high-temperature alteration. These losses and gains are broadly similar to those summarised for modern low-temperature seawater–basalt interaction by Thompson et al. (1983), but differ in several details (Si, Mn, Mg). This shows that modern deep-water models should not be applied to models for early seawater evolution, because shallow-water extrusion and alteration were probably much more important before 2000 Ma.

13. Conclusions

(1) Ongeluk and Hekpoort lavas of the greater Transvaal Basin together represent a major Palaeoproterozoic volcanic episode, extrusions covered most of the Kaapvaal Craton. The only significant primary geochemical variation within the Ongeluk magma is in Cr content, which may be related to contamination by Cr-rich material. The basaltic andesite lavas were derived from an anomalous segment of the Kaapvaal lithosphere with a complex history involving high U/Pb, high Rb/Sr and near-chondritic Sm/Nd ratios.

(2) The major and trace element data for Ongeluk pillow lavas, hyaloclastites and massive lavas all conform to a model envisaging major interaction with seawater at depths between 400 and 1680 m soon after extrusion. Two classes of alteration are recognised: class 2 high-temperature typified by pillow cores; and class 3 low-temperature best developed in hyaloclastites. Class 1 supercritical alteration did not take place due to water depths less than 2286 m. While no exact modern analogue exists, several similarities were found with deep- and shallow-seafloor alteration described in the literature.

(3) Sr isotope data require a two-phase alteration model. In the first phase Sr isotope ratios are lowered by interaction with the Ongeluk sea at the time of extrusion. The second phase, involving losses and gains of either or both Rb and Sr, probably occurred about 1000 Ma after extrusion and affected only a few samples characterised by high Ca/Sr ratios.

(4) Pb isotope data show evidence for changes in U/Pb ratios during only the first phase, while no evidence for the second phase was found. Modelling of seawater alteration yields such small changes in Pb isotope ratios, that the 2222 ± 13 Ma Pb–Pb whole-rock isochron age obtained in this work is regarded as a reliable refinement of earlier Rb–Sr and Pb–Pb ages for the origin of the Ongeluk lavas.

(5) The seawater alteration exchanged major amounts of elements such as alkalis, alkaline earths, Fe, Mg and Mn with the Ongeluk ocean. Models for chemical evolution of the early ocean should not overlook the differences between modern deep water interactions and the shallow-water alteration documented in this work.

Acknowledgements

This work was initiated as a Collaborative Science Project, funded by the South African Foundation for Research Development, and this paper is based on the PhD thesis of SS, submitted to the University of Natal, Durban. We are grateful to Samanacor for additional financial support. XRF analyses were done in the Geology Departments of the Universities of Stellenbosch and Natal (Pietermaritzburg). J.P. Engelbrecht kindly allowed us to use his geochemical data on Hekpoort and Ongeluk lavas. Electron probe analyses were made in the Department of Geosciences, University of Cape Town. Isotope analyses were done at the CSIR and at the Open University. DHC thanks the Institute of Crystallography and Petrography, ETH Zürich for providing a peaceful haven in which to complete this paper.

References

Alt, J.C. and Honnorez, J., 1984. Alteration of the upper oceanic crust, DSDP site 417; mineralogy and chemistry. Contrib. Mineral. Petrol., 87: 149–169.

Armstrong, R.A., 1987. Geochronological Studies on Archean and Proterozoic Formations of the Namaqua Front and Possible Correlates on the Kaapvaal Craton. Ph.D. thesis (unpubl.), Univ. Witwatersrand, Johannesburg, 274 pp.

Beukes, N.J. and Smit, C.A., 1987. New evidence for thrust faulting in Griqualand West, South Africa: implications for stratigraphy and the age of red beds. S. Afr. J. Geol., 90: 378–394.

Brevart, O., Dupre, B. and Allegre, C.J., 1981. Metallogenesis at spreading centres: Lead isotope systematics for sulphides, manganese-rich crusts, basalts and sediments from the Cyamex and Alvin areas (East Pacific Rise). Econ. Geol., 76: 1205–1210.

Cann, J.R., 1979. Metamorphism in the ocean crust. In: M. Talwani, C.G. Harrison and D.E. Hayes (Editors), Deep Drilling Results in the Atlantic Ocean: Ocean Crust. American Geophysical Union, Washington, pp. 230–238.

Cathelineau, M. and Nieva, D., 1985. A chlorite solid solution geothermometer. The Los Azufres (Mexico) geothermal system. Contrib. Mineral. Petrol., 91: 235–244.

Cornell, D.H., Hawkesworth, C.J., Van Calsteren, P. and Scott, W.D., 1986. Sm–Nd study of Precambrian crustal development in the Prieska–Copperton region, Cape Province. Trans. Geol. Soc. S. Afr., 89: 17–28.

Cornell, D.H., Humphreys, H., Theart, H.F.J. and Scheepers, D.J., 1992. A collision-related pressure–temperature–time path for Prieska Copper Mine, Namaqua–Natal tectonic province, South Africa. Precambrian Res., 59: 43–71.

Cornell, D.H., Armstrong, R.A. and Walraven, F., 1996. The Hartley Basalt Formation: geochemistry and geochronology of a 1928 Ma volcanic suite and its relation to the breakup of the Kaapvaal Craton. S. Afr. J. Geol., in press.

Dixon, R.D., 1989. Sugilite and associated metamorphic silicate minerals from Wessels Mine, Kalahari Manganese Field. Geol. Surv. Bull. S. Afr., 93, 47 pp.

Eglington, B.M. and Harmer, R.E., 1991. GEODATE: a program for the processing and regression of isotope data using IBM-compatible microcomputers. CSIR Manual EMA-H, 57 pp.

Eglington, B.M. and Kerr, A., 1989. Rb–Sr and Pb–Pb geochronology of Proterozoic intrusions from the Scottburgh area of southern Natal. S. Afr. J. Geol., 92: 393–399.

Engelbrecht, J.P., 1986. Die Bosveld Kompleks en sy Vloergesteentes in die Omgewing van Nietverdiend, Wes-Transvaal. Unpubl. Ph.D. thesis, Univ. Pretoria, 327 pp.

Faure, G., 1986. Principles of Isotope Geology. 2nd ed., Wiley, New York, 589 pp.

Gill, J.B., 1981. Orogenic Andesites and Plate Tectonics. Springer-Verlag, Berlin, 358 pp.

Grobler, N.J. and Botha, B.J.V., 1976. Pillow-lavas and hyaloclastite in the Ongeluk Andesite Formation in a road-cutting west of Griquatown, South Africa. Trans. Geol. Soc. S. Afr., 79: 53–57.

Hamilton, P.J., 1977. Sr-isotope and trace-element studies of the Great Dyke and Bushveld mafic phase and their relation to early Proterozoic magma genesis in Southern Africa. J. Petrol., 18: 24–52.

Harmer, R.E. and Sharp, M.R., 1985. Field relations and strontium isotope systematics of the marginal rocks of the Bushveld Complex. Econ. Geol., 80: 813–837.

Harmer, R.E. and von Gruenewaldt, G., 1991. A review of magmatism associated with the Transvaal Basin—implications for its tectonic setting. S. Afr. J. Geol., 94: 104–122.

Henderson, P., 1982. Inorganic Geochemistry. Pergamon, Oxford, 353 pp.

Hey, M.H., 1954. A new review of the chlorites. Mineral. Mag., 30: 277.

Hughes, C.J., 1973. Spilites, keratophyres, and the igneous spectrum. Geol. Mag., 109: 513–527.

Humphris, S.E. and Thompson, G., 1978. Trace element mobility during hydrothermal alteration of oceanic basalts. Geochim. Cosmochim. Acta, 42: 127–136.

Irvine, T.N. and Baragar, W.R.A., 1971. A guide to the chemical classification of the common volcanic rocks. Can. J. Earth Sci., 8: 523–548.

Jasinski, A.W., Baker, J.H. and De Groot, P.A., 1985. Thermodynamic aspects of the Mg–chlorite–alkali feldspar–sericite–kaolinite system: Applications to the fossil sub-seafloor hydrothermal system at Hjulsjö, Bergslagen, Sweden. GUA Papers of Geology, Ser. 1, 21, 204 pp.

Key, R.M., 1983. The geology of the area around Gaborone and Lobatse, Kweneng, Kgatleng, Southern and South East Districts. Geol. Surv. Botswana, Dist. Mem., 5, 230 pp.

Key, R.M. and Rundle, C.C., 1981. The regional significance of new isotopic ages from Precambrian windows through the 'Kalahari Beds' in northwestern Botswana. Trans. Geol. Soc. S. Afr., 84. 51–66.

Kristmansdottir, H., 1983. Chemical evidence from Icelandic geothermal systems as compared to submarine geothermal systems. In: P.A. Rona, K. Boström, L. Laubier and K.L. Smith (Editors), Hydrothermal Processes at Seafloor Spreading Centres. NATO Conference Series, IV. Marine Sciences, Plenum Press, New York, pp. 291–320.

MacFarlane, A.W. and Holland, H.D., 1991. The timing of alkali metasomatism in paleosols. Can. Mineral., 29: 1043–1050.

MacLean, W.H. and Kranidiotis, P., 1987. Immobile elements as monitors of mass transfer in hydrothermal alteration: Phelps Dodge massive sulfide deposit, Matagami, Quebec. Econ. Geol., 82: 951–962.

Marsh, J.S., 1987. Basalt geochemistry and tectonic discrimination within continental flood basalt provinces. J. Volcanol. Geotherm. Res., 32: 35–49.

Michard, A. and Albarède, F., 1986. The REE content of some hydrothermal fluids. Chem. Geol., 55: 51–60.

Mottl, M.J., 1983. Metabasalts, axial hot springs, and the structure of hydrothermal systems at mid-ocean ridges. Geol. Soc. Am. Bull., 94: 161–180.

Norrish, K. and Hutton, J.T., 1969. An accurate X-ray spectrographic method for the analysis of a wide range of geological samples. Geochim. Cosmochim. Acta, 33: 431–453.

Pearce, J.A., 1983. The role of sub-continental lithosphere in magma genesis at destructive plate margins. In: C.J. Hawkesworth and M.J. Norry (Editors), Continental Basalts and Mantle Xenoliths. Shiva, Cambridge, Mass., pp. 230–249.

Sabine, P.A., 1989. Setting standards in petrology: The Commission on systematics in petrology. Episodes, 12: 84–86.

SACS—South African Committee for Stratigraphy, 1980. Stratigraphy of South Africa. Part 1 (Comp. L.E. Kent). Lithostratigraphy of the Republic of South Africa, South West Africa/Namibia and the Republics of Bophuthatswana, Transkei and Venda. Handbook Geol. Surv. S. Afr., 8, 690 pp.

Schade, J., Cornell, D.H. and Theart, H.F.J., 1989. Rare Earth element and isotopic evidence for the genesis of the Prieska massive sulfide deposit, South Africa. Econ. Geol., 84: 49–63.

Schütte, S.S., 1992. Ongeluk Volcanism in Relation to the Kalahari Manganese Deposits. Unpubl. PhD thesis, Univ. Natal, 255 pp.

Stacey, J.S. and Kramers, J.D., 1975. Approximation of terrestrial lead isotope evolution by a two-stage model. Earth Planet. Sci. Lett., 26: 207–221.

Steiger, R.H. and Jäger, E., 1977. Subcommission on geochronology: convention on the use of decay constants in geo- and cosmochronology. Earth Planet. Sci. Lett., 36: 359–362.

Thompson, R.N., Morrison, M.A., Hendry, G.L. and Parry, S.J., 1983. An assessment of the relative roles of crust and mantle in magma genesis—an elemental approach. Philos. Trans. R. Soc. London, A310: 549–590.

Turner, A.M., 1992. Zinc–Lead Mineralization at Pering Mine in the Griqualand West Sub-Basin—An Isotopic Study. Unpubl. MSc thesis, Univ. Natal.

Veizer, J., Hoefs, J., Ridler, R.H., Jensen, L.S. and Lowe, D.R., 1989. Geochemistry of Precambrian carbonates, I. Archean hydrothermal systems. Geochim. Cosmochim. Acta, 53: 845–857.

Vidal, P. and Clauer, N., 1981. Pb and Sr systematics of some basalts and sulphides from the East Pacific Rise at 21°N (project RITA). Earth Planet. Sci. Lett., 55: 237–246.